# Long-lived states of antiprotonic lithium $\bar{p}\mathrm{Li}^+$ produced in $\bar{p}+\mathrm{Li}$ collisions

Kazuhiro Sakimoto

*Institute of Space and Astronautical Science, Japan Aerospace Exploration Agency, Yoshinodai 3-1-1, Chuo-ku, Sagamihara,*
*Kanagawa 252-5210, Japan*

Antiproton capture by lithium atoms ($\bar{p} + \mathrm{Li} \rightarrow \bar{p}\mathrm{Li}^+ + e$) is investigated at collision energies from 0.01 to 10 eV by using a semiclassical (also know as quantum-classical hybrid) method, in which the radial distance between the antiproton and the $\mathrm{Li}^+$ ion is treated as a classical variable, and the other degrees of freedom are described by quantum mechanics. Analyzing the wave packet of the emitted electrons and making use of the energy conservation rule enable us to calculate the state distribution of the produced antiprotonic lithium $\bar{p}\mathrm{Li}^+$ atoms and also to distinguish between the capture and ionization ($\rightarrow \bar{p} + \mathrm{Li}^+ + e$) channels at collisional energies above the ionization threshold. This method is tested for the capture of negative muons by hydrogen atoms, which was rigorously investigated in previous quantum mechanical studies. Most of the $\bar{p}\mathrm{Li}^+$ atoms produced in $\bar{p} + \mathrm{Li}$ are found to be sufficiently stable against Auger decays and are experimentally observable as long-lived states. The present system bears close similarities to the system of $\bar{p} + \mathrm{He}(2S)$. It is therefore expected that long-lived antiprotonic helium $\bar{p}\mathrm{He}^+$ atoms can be efficiently produced in the $\bar{p}$ capture by metastable $\mathrm{He}(2\,^3S)$ atoms.

## I. INTRODUCTION

Special attention is payed to long-lived states of antiprotonic helium atoms ($\bar{p}\mathrm{He}^+$) produced in the capture of antiprotons ($\bar{p}$) by helium atoms [1–3]. Delayed annihilation of $\bar{p}$ in gaseous, liquid, and solid helium is attributed to the existence of the long-lived $\bar{p}\mathrm{He}^+$ atoms [1]. Furthermore, a spectroscopic measurement of the $\bar{p}\mathrm{He}^+$ atoms is an effective means of determining the fundamental physical constants such as the $\bar{p}$ mass [2,3]. The $\bar{p}\mathrm{He}^+$ states produced in the capture reaction are embedded in the continuum $\bar{p}\mathrm{He}^{2+} + e$, and are usually unstable due to a prompt Auger transition. However, if the $\bar{p}$ orbital in $\bar{p}\mathrm{He}^+$ has a large principal quantum number $N$ and, additionally, an angular momentum quantum number $L$ close to the maximum $N - 1$ (i.e., a circular or near-circular state), the Auger transition requires a large angular momentum change and hence can be suppressed [4–7]. This mechanism of Auger suppression was proposed by Condo [4] and Russell [5], and is considered to be the reason for the existence of long-lived $\bar{p}\mathrm{He}^+$ atoms. As for the $\bar{p}$ capture by other rare-gas atoms, however, no positive evidence was experimentally found for long-lived antiprotonic atoms [1,8]. For these targets, although it was estimated that the probability of capture into the near-circular states should be negligible [9], the full details are still unknown.

Ahlrichs *et al.* [10] calculated the Born-Oppenheimer (BO) potentials of the $\bar{p} + \mathrm{Li}^+$ and $\bar{p} + \mathrm{Li}^{2+}$ systems and suggested that the Auger process of the circular state ($L = N - 1$) in antiprotonic lithium atoms ($\bar{p}\mathrm{Li}^+$) can be much slower than that in $\bar{p}\mathrm{He}^+$. A similar study was made by Révai and Belyaev [11]. Shimamura *et al.* [12] further pointed out that the Auger transition can also be strongly suppressed for much lower $L$ other than for $L \sim N - 1$. Thus, one can expect a more enlarged possibility of producing long-lived antiprotonic atoms in the $\bar{p} + \mathrm{Li}$ collisions as compared with the case of $\bar{p} + \mathrm{He}$. Nevertheless, in confirmation of the experimental observability of $\bar{p}\mathrm{Li}^+$ as the quasibound system, it is very important to know the precise distribution of the $\bar{p}\mathrm{Li}^+$ states produced in the capture process and then to investigate the stability

of the individual states. Cohen made a theoretical study of the capture in $\bar{p} + \mathrm{Li}$ by using a fermion-molecular-dynamics (FMD) method [13]. Unfortunately, only the total capture cross sections were calculated in his study. At the present time, no theoretical calculation has been performed for the state distribution of the $\bar{p}\mathrm{Li}^+$ products in the $\bar{p} + \mathrm{Li}$ collisions.

Recently, several quantum mechanical (QM) calculations were carried out to provide the product-state distribution in the captures by H, $\mathrm{He}^+$, and He [14–17]. However, the QM calculation becomes exceedingly troublesome for the $\bar{p} + \mathrm{Li}$ system because the diffuse orbital of the valence $2s$ electron is involved. In the capture reaction, the binding energy of the $\bar{p}$ orbital in the $\bar{p}\mathrm{Li}^+$ product likely matches that of the valence electron in the Li target. Then, the produced $\bar{p}\mathrm{Li}^+$ states consist of very high principal quantum numbers $N \sim 60$, which further complicate a sophisticated QM treatment. Another possibility of performing a reasonable study for such cases is to employ a semiclassical (SC) approximation, in which the electron motion is described by quantum mechanics, and the heavy particle motion is assumed to be classical.[1] The SC calculations of the capture process were carried out for a H target by Kwong *et al.* [18] and the present author [19,20]. Although the SC method succeeded in reproducing the total capture cross sections obtained by previous QM calculations [20], it was unable to provide the product-state distribution. A previous study [20] has confirmed, however, that the mechanism of electron emission can be properly understood within the framework of the SC method. It suggests that the SC method might also be usable for getting information of the product-state distribution if one made good use of the conservation laws of angular momentum and of energy.

In this paper, an SC method is developed which allows the calculation of the state distributions of the antiprotonic atoms produced in $\bar{p}$ capture by atoms. The results are presented for

------

[1]This approach is also referred to as a quantum-classical hybrid approximation

the capture process $\bar{p} + \text{Li} \rightarrow \bar{p}\text{Li}^+ + e$, and the possibility of the formation of long-lived $\bar{p}\text{Li}^+$ atoms in this process is discussed. The cross section for the ionization process $\bar{p} + \text{Li} \rightarrow \bar{p} + \text{Li}^+ + e$ is also calculated. A further comment is provided on the long-lived $\bar{p}\text{He}^+$ atoms produced in $\bar{p}$ capture by metastable $\text{He}(2\,^3S)$ atoms.

## II. THEORY

### A. Interaction

We assume that the $\bar{p} + \text{Li}$ system can be regarded as a three-body $(\bar{p}, \text{Li}^+, e)$ problem, and that the interaction is given by the sum of the two-body terms; that is,

$$V = V_{e\text{-Li}^+}(r) + \frac{1}{|\mathbf{R} - \mathbf{r}|} + V_{\bar{p}\text{-Li}^+}(R), \qquad (1)$$

where $\mathbf{r}$ is the position vector of $e$ from $\text{Li}^+$, and $\mathbf{R}$ is that of $\bar{p}$ from $\text{Li}^+$. Thus, in the present study, the processes related to multielectron emission and to inner-electron excitation are neglected. It is naturally expected that these processes occur much less frequently than valence-electron emission. The effect that the $\text{Li}^+$ core is not a point charge is included in the two-body local potentials $V_{e\text{-Li}^+}(r)$ and $V_{\bar{p}\text{-Li}^+}(R)$, which behave as $V_{e\text{-Li}^+}(r) = -1/r$ and $V_{\bar{p}\text{-Li}^+}(R) = -1/R$ at large distances. For the valence electron in Li, Peach *et al.* [21] provided a semiempirical-model potential, which gives the $2s$-state energy $\mathcal{E}_{\text{Li}} = -5.39$ eV. This potential was adopted for $V_{e\text{-Li}^+}(r)$. The relative motion between $\bar{p}$ and $\text{Li}^+$ is determined by the potential $V_{\bar{p}\text{-Li}^+}(R)$. In the case of $\bar{p}\text{He}^+$, the BO approximation is appropriate for the high $\bar{p}$ orbital motion, which can thus be regarded as the molecular vibration [22]. For this reason, the BO energies, calculated by Ahlrichs *et al.* [10], were used for obtaining $V_{\bar{p}\text{-Li}^+}(R)$. The same type of approximation for the interaction was employed by Tong *et al.* in the study of the $\bar{p}$ capture by He [15].

### B. Semiclassical method

In the present SC method, differently from the ordinary method, only the radial distance $R$ is treated as a classical variable, and all the other motions are described by quantum mechanics [23]. For the quantum mechanical part of the Hamiltonian, we consider

$$\tilde{H} = \frac{\tilde{\mathbf{L}}^2}{2m_R R^2} - \frac{1}{2m_r r} \frac{\partial^2}{\partial r^2} r + \frac{\tilde{\mathbf{l}}^2}{2m_r r^2} + V_0, \qquad (2)$$

where $\tilde{\mathbf{L}}$ is the angular momentum operator of $\bar{p}\text{Li}^+$, $\tilde{\mathbf{l}}$ is the electron angular momentum operator, $m_R$ and $m_r$ are the reduced masses of $\bar{p} + \text{Li}^+$ and $e + \text{Li}^+$, respectively, and

$$V_0 = V_{e\text{-Li}^+}(r) + \frac{1}{|\mathbf{R} - \mathbf{r}|} \qquad (3)$$

is the interaction associated with the quantum mechanical motion. Here and in the following, we use a.u. unless otherwise stated. The advantage of the present SC treatment is that the conservation of the total angular momentum $\tilde{\mathbf{J}} = \tilde{\mathbf{L}} + \tilde{\mathbf{l}}$ is taken into account quantum mechanically. This allows us to directly calculate the angular momentum distribution of the products after the collisions. In the coordinate system $(\mathbf{R}, \mathbf{r})$ employed in Eq. (2), the cross term actually arises in the kinetic energy

operators (known as the mass polarization effect in the atomic structure [24]). However, because the $\bar{p}$ mass is much smaller than the $\text{Li}^+$ mass, we can practically neglect the cross term (cf. Sec. III B).

The time-dependent Schrödinger equation in the SC method becomes

$$i \frac{\partial}{\partial t} \Psi^{JM}(\hat{\mathbf{R}}, \mathbf{r}, t) = \tilde{H} \Psi^{JM}(\hat{\mathbf{R}}, \mathbf{r}, t). \qquad (4)$$

For the convenience of numerical calculations, the body-fixed (BF) frame in which the $z$ axis is chosen along $\mathbf{R}$ is introduced. Using $\tilde{\mathbf{L}}^2 = (\tilde{\mathbf{J}} - \tilde{\mathbf{l}})^2$ in the BF frame, we can write the total wave function $\Psi^{JM}(\hat{\mathbf{R}}, \mathbf{r}, t)$ in the form [23]

$$\Psi^{JM}(\hat{\mathbf{R}}, \mathbf{r}, t) = \frac{1}{r} \sum_{\lambda \geqslant 0} \mathcal{D}^J_{M\lambda}(\hat{\mathbf{R}}) \psi^{J\lambda}(\mathbf{r}, t)$$
$$\times \exp\left[-i \int^t \frac{J(J+1)}{2m_R R^2} dt'\right], \qquad (5)$$

where $(J, M)$ are the total angular momentum quantum numbers, $\lambda$ is the magnetic quantum number of $\tilde{l}_z = \tilde{J}_z$, and

$$\mathcal{D}^J_{M\lambda}(\hat{\mathbf{R}}) = \left[\frac{2J+1}{8\pi(1+\delta_{\lambda 0})}\right]^{1/2}$$
$$\times [D^J_{M\lambda}(\hat{\mathbf{R}}) + (-1)^\lambda D^J_{M-\lambda}(\hat{\mathbf{R}})]^* \qquad (6)$$

is the symmetrized and normalized form of the Wigner's rotation matrix element $D^J_{M\lambda}(\hat{\mathbf{R}})$.

### C. Initial condition and classical trajectory

The initial condition of the wave function $\psi^{J\lambda}(\mathbf{r}, t)$ in Eq. (5) can be chosen as [20]

$$\psi^{J\lambda}(\mathbf{r}, t = 0) = \chi(\mathbf{r}; R_0)\, \delta_{\lambda 0}, \qquad (7)$$

where $\chi(\mathbf{r}; R_0)$ represents the BO state of $\bar{p} + \text{Li}$, correlating with the ground state of Li, and $R_0 = R(t = 0)$ is the initial radial distance. The BO wave function $\chi(\mathbf{r}; R)$ is given by

$$\left[-\frac{1}{2m_r r} \frac{\partial^2}{\partial r^2} r + \frac{\tilde{\mathbf{l}}^2}{2m_r r^2} + V_0\right] \frac{1}{r} \chi(\mathbf{r}; R) = \mathcal{E}_{\text{BO}}(R) \frac{1}{r} \chi(\mathbf{r}; R). \qquad (8)$$

The BO electronic energy $\mathcal{E}_{\text{BO}}(R)$ has the limit $\mathcal{E}_{\text{BO}}(\infty) = \mathcal{E}_{\text{Li}} = -I$, with $I$ being the first ionization energy of Li.

As was discussed in the previous SC study [20], the time dependence of the variable $R(t)$ can be given by the following classical equation of motion:

$$E + \mathcal{E}_{\text{Li}} = \frac{m_R}{2}\left(\frac{dR}{dt}\right)^2 + U_{\text{eff}}(R), \qquad (9)$$

where $E$ is the collision energy and

$$U_{\text{eff}}(R) = \frac{(J + 1/2)^2}{2m_R R^2} + \mathcal{E}_{\text{BO}}(R) + V_{\bar{p}\text{-Li}^+}(R) \qquad (10)$$

is the effective potential. The $\bar{p} + \text{Li}$ adiabatic potential $U_{\text{ad}}(R) = \mathcal{E}_{\text{BO}}(R) + V_{\bar{p}\text{-Li}^+}(R)$ has the asymptotic $(R \rightarrow \infty)$ form

$$U_{\text{ad}}(R) \rightarrow \mathcal{E}_{\text{Li}} - \frac{\alpha}{2R^4}, \qquad (11)$$

where $\alpha$ is the polarizability of Li.

### D. Capture state analysis

In the present treatment, the trajectory $R(t)$ given by Eq. (9) never exhibits capture behavior: $R$ always diverges at $t \rightarrow \infty$. However, it is found that the probability of electron emission can be obtained with reasonable accuracy by using this trajectory [20]. Here, we consider the collision energies to be below the first ionization threshold of Li (i.e., $E < I$). Then, the electron emission probability is just equal to the capture probability, and the whole of the angular-momentum and kinetic-energy distribution of the emitted electrons can be related to the state distribution of the produced $\bar{p}Li^+$ atoms.

To discuss the product-state distributions, one needs to express the total wave function $\Psi^{JM}$ in the space-fixed (SF) frame; that is,

$$\Psi^{JM}(\hat{\mathbf{R}},\mathbf{r}',t) = \frac{1}{r}\sum_{Ll} \mathcal{Y}_{Ll}^{JM}(\hat{\mathbf{R}},\hat{\mathbf{r}}') f_{Ll}^J(r,t)$$
$$\times \exp\left[-i\int^t \frac{J(J+1)}{2m_R R^2}dt'\right], \quad (12)$$

where $\mathbf{r}'$ is the electron coordinates represented in the SF frame, $L$ is the angular momentum quantum number of $\bar{p}Li^+$, $l$ is the electronic quantum number, the summation is restricted to $(-1)^{J+L+l} = 1$ owing to the parity conservation, and $\mathcal{Y}_{Ll}^{JM}(\hat{\mathbf{R}},\hat{\mathbf{r}}')$ is the eigenfunction of the total angular momentum given by

$$\mathcal{Y}_{Ll}^{JM}(\hat{\mathbf{R}},\hat{\mathbf{r}}') = \sum_{M_L m}(LM_L lm|JM)Y_{LM_L}(\hat{\mathbf{R}})Y_{lm}(\hat{\mathbf{r}}'), \quad (13)$$

with the Clebsch-Gordan coefficient $(LM_L lm|JM)$ and the spherical harmonics $Y_{LM_L}$. We notice the following relation between the SF and BF angular basis functions [25]:

$$\mathcal{Y}_{Ll}^{JM}(\hat{\mathbf{R}},\hat{\mathbf{r}}') = \sum_{\lambda \geqslant 0} U_{L\lambda}^{Jl}\mathcal{D}_{M\lambda}^J(\hat{\mathbf{R}})Y_{l\lambda}(\hat{\mathbf{r}}), \quad (14)$$

with the orthogonal transformation matrix element

$$U_{L\lambda}^{Jl} = \left(\frac{2L+1}{2J+1}\right)^{1/2}(L0l\lambda|J\lambda)\frac{1+(-1)^{J+L+l}}{[2(1+\delta_{\lambda 0})]^{1/2}}. \quad (15)$$

Then, we can show that the wave function $f_{Ll}^J(r,t)$ in Eq. (12) is calculated from $\psi^{J\lambda}(\mathbf{r},t)$ in Eq. (5) by using

$$f_{Ll}^J(r,t) = \sum_{\lambda \geqslant 0} U_{L\lambda}^{Jl}\langle Y_{l\lambda}|\psi^{J\lambda}(t)\rangle_r. \quad (16)$$

For a sufficiently large $r = r_0$, the wave function $f_{Ll}^J(r_0,t)$ represents the motion of emitted electrons and can be expressed in the wave-packet form as

$$f_{Ll}^J(r_0,t) = \int g_{Ll}^J(r_0,\epsilon)C_{Ll}^J(\epsilon)e^{-i\epsilon t}d\epsilon, \quad (17)$$

where $g_{Ll}^J(r,\epsilon)$ is the out-going stationary wave function of the electron having the kinetic energy $\epsilon$ and satisfying the unit-energy normalization. From this definition, the coefficient $C_{Ll}^J(\epsilon)$ is related to the probability density by

$$\frac{dP_{Ll}^J}{d\epsilon} = \left|C_{Ll}^J(\epsilon)\right|^2. \quad (18)$$

For the numerical calculation of $|C_{Ll}^J(\epsilon)|^2$, it is convenient to analyze the outgoing flux of electrons [26,27]. This analysis leads to

$$\frac{dP_{Ll}^J}{d\epsilon} = \frac{1}{m_r}\text{Im}\left[(A_{Ll}^J)^*\frac{dA_{Ll}^J}{dr}\right]_{r=r_0}, \quad (19)$$

where

$$A_{Ll}^J(r,\epsilon) = \frac{1}{\sqrt{2\pi}}\int e^{i\epsilon t} f_{Ll}^J(r,t)dt. \quad (20)$$

Integration of $dP_{Ll}^J/d\epsilon$ over $\epsilon$ and the summation over $l$ yield the probability of capture into the $L$ state:

$$P_L^J = \sum_l \int \frac{dP_{Ll}^J}{d\epsilon}d\epsilon = \frac{1}{m_r}\sum_l \int \text{Im}\left[(f_{Ll}^J)^*\frac{df_{Ll}^J}{dr}\right]_{r=r_0} dt. \quad (21)$$

Further summation over $L$ gives the total capture probability:

$$P^J = \sum_L P_L^J = \frac{1}{m_r}\sum_{\lambda \geqslant 0}\int \text{Im}\left\langle \psi^{J\lambda}\left|\frac{d\psi^{J\lambda}}{dr}\right.\right\rangle_{r=r_0} dt. \quad (22)$$

In order to obtain the relation between the electron energy $\epsilon$ and the internal state of the $\bar{p}Li^+$ atom, we apply the conservation rule of the total energy $E_{tot}$; that is,

$$E_{tot} = E + \mathcal{E}_{Li} = E_{NL} + \epsilon, \quad (23)$$

where $E_{NL}$ is the energy of the vibrational motion supported by the potential $V_{\bar{p}\text{-Li}^+}(R)$. The principal quantum number $N$ of the $\bar{p}$ orbital in $\bar{p}Li^+$ can be defined by $N = v + L + 1$, with $v$ being the classical counterpart of the vibrational quantum number; namely,

$$v + \frac{1}{2} = \frac{\sqrt{2m_R}}{\pi}\int_{R_1}^{R_2}\left[E_{NL} - \frac{(L+1/2)^2}{2m_R R^2}\right.$$
$$\left. - V_{\bar{p}\text{-Li}^+}(R)\right]^{1/2} dR, \quad (24)$$

where $R_1$ and $R_2$ are the turning points of the vibrational motion. It should be noted that $N$ is a continuous variable in the present treatment. By using Eq. (23), we can have

$$\frac{dP_{Ll}^J}{dN} = \left|\frac{\partial E_{NL}}{\partial N}\right|\frac{dP_{Ll}^J}{d\epsilon}, \quad (25)$$

and the derivative $\partial E_{NL}/\partial N$ is easily calculated from Eq. (24). We define the probability (density) of the capture into the $(N,L)$ state as

$$\frac{dP_L^J}{dN} = \sum_l \frac{dP_{Ll}^J}{dN}. \quad (26)$$

The idea of utilizing the energy conservation in the SC method was adopted by Ovchinnikov and Macek [28] in the calculation of $\bar{p}$ capture by H. However, the addition of the angular momenta and the relation between the BF and SF frames were not properly taken into account in their study.

The total capture cross section is given by

$$\sigma = \frac{\pi}{2m_R E}\Omega, \quad (27)$$

with

$$\Omega = \sum_J (2J+1) P^J. \tag{28}$$

We define the energy distribution of the emitted electrons by

$$F(\epsilon) = \frac{1}{\Omega} \sum_{JLl} (2J+1) \frac{dP_{Ll}^J}{d\epsilon} \tag{29}$$

and the state distributions of the products $\bar{p}\mathrm{Li}^+$ by

$$F(N,L) = \frac{1}{\Omega} \sum_J (2J+1) \frac{dP_L^J}{dN}, \tag{30}$$

$$F(N) = \frac{1}{\Omega} \sum_{JL} (2J+1) \frac{dP_L^J}{dN}, \tag{31}$$

$$F(L) = \frac{1}{\Omega} \sum_J (2J+1) P_L^J. \tag{32}$$

### E. Collision energies above the ionization threshold

When the collision energy is above the first ionization threshold (i.e., $E > I$), the ionization channel ($\rightarrow \bar{p} + \mathrm{Li}^+ + e$) becomes open. In the present study, we can distinguish between the capture and ionization channels according to $\epsilon > E + \mathcal{E}_{\mathrm{Li}}$ or $\epsilon < E + \mathcal{E}_{\mathrm{Li}}$. At collision energies $E > I$, the total capture probability thus becomes

$$P^J = \sum_{Ll} \int_{E+\mathcal{E}_{\mathrm{Li}}}^{\infty} \frac{dP_{Ll}^J}{d\epsilon} d\epsilon \tag{33}$$

and the total ionization probability is given by

$$P_{\mathrm{ion}}^J = \sum_{Ll} \int_0^{E+\mathcal{E}_{\mathrm{Li}}} \frac{dP_{Ll}^J}{d\epsilon} d\epsilon. \tag{34}$$

The total ionization cross section $\sigma_{\mathrm{ion}}$ is defined in the same way as in Eq. (27).

## III. NUMERICAL CALCULATION

### A. Numerical consideration

The BO electronic energies $\mathcal{E}_{\mathrm{BO}}(R)$ of the $\bar{p} + \mathrm{Li}$ system was calculated by using the grid-representation method based on orthogonal polynomials [20,23]: the Laguerre polynomials with 150 points for the $r$ coordinate and the Legendre polynomials with three points for the angular ($\theta = \cos^{-1} \hat{R} \cdot \hat{r}$) coordinate. This set of parameters gives the polarizability of Li, $\alpha = 168$ a.u., which is very close to the accurate value 162 a.u. [29]. In Fig. 1, the electronic energy $\mathcal{E}_{\mathrm{BO}}(R)$ and the $\bar{p} + \mathrm{Li}$ adiabatic potential $U_{\mathrm{ad}}(R)$ are plotted and compared with those of the $\bar{p} + \mathrm{H}$ system. For reference, several energy levels $E_{NL}$ of the $\bar{p}\mathrm{Li}^+$ atom are shown for $L = 50$. Because $V_0 \rightarrow \mathbf{R} \cdot \mathbf{r}/r^3$ in the limit $r \rightarrow \infty$, an infinite series of electronic bound states exists in Eq. (8) at $R > 0.639$ a.u. [30], and $\mathcal{E}_{\mathrm{BO}}(R)$ should be zero at $R = 0.639$ a.u. The present calculation provides $R = 0.949$ a.u. for such a critical point. If the distance is $R \lesssim 1$ a.u., it is hard to determine numerically the accurate value of $\mathcal{E}_{\mathrm{BO}}(R)$, which is very close to zero.
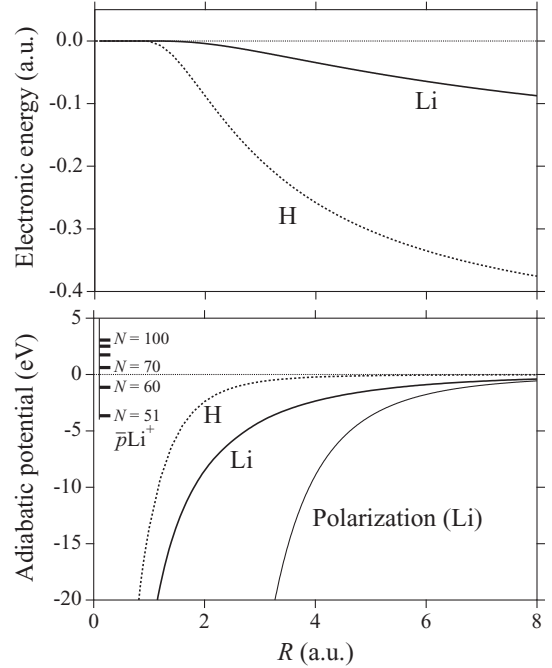


FIG. 1. Electronic energies $\mathcal{E}_{\mathrm{BO}}(R)$, adiabatic potential $U_{\mathrm{ad}}(R) - \mathcal{E}_{\mathrm{Li}}$, and polarization potential $-\alpha/(2R^4)$ of $\bar{p} + \mathrm{Li}$. Electronic energies and adiabatic potential of $\bar{p} + \mathrm{H}$ are also shown. The horizontal bars are the energy levels $E_{NL} - \mathcal{E}_{\mathrm{Li}}$ of $\bar{p}\mathrm{Li}^+$ for $L = 50$.

However, the accurate value is not so important in the present study since the term $V_{\bar{p}\text{-}\mathrm{Li}^+}(R)$ dominates the $\bar{p} + \mathrm{Li}$ adiabatic potential $U_{\mathrm{ad}}(R)$ at $R < 2$ a.u. In the trajectory calculation, $\mathcal{E}_{\mathrm{BO}}(R) = 0$ is assumed at $R < 0.949$ a.u., as in the previous treatment [20].

For the numerical calculation of the wave function $\psi^{J\lambda}(\mathbf{r},t)$ in Eq. (5), the grid-representation method was also employed. The details are given in Ref. [23]. Depending on whether $\lambda = $ even or odd, the Legendre or Gegenbauer polynomials with three points were adopted for the $\theta$ coordinate. For the electron motion, since it was necessary to accurately evaluate an outgoing flux at $r = r_0 = 45$ a.u., the Chebyshev polynomials with 530 points were adopted in the range $0 \leqslant r \leqslant 80$ a.u., and the complete absorbing potential [23] was applied to avoid reflection from the outer boundary. The channels of $\lambda = 0$ and 1 were coupled, and the initial distance was chosen as $R_0 = 5$ a.u. The SC calculation was carried out at collision energies $0.01 \leqslant E \leqslant 10$ eV. The total angular momenta considered in the calculation are $J \leqslant 33$ at $E = 0.01$ eV and $J \leqslant 125$ at $E = 10$ eV.

The existence of the unphysical 1s state supported by the potential $V_{e\text{-}\mathrm{Li}^+}(r)$ may have an adverse effect on the present results. One can remove this effect by applying the projection operator $\tilde{P} = 1 - |1s\rangle\langle 1s|$, with $|1s\rangle$ representing the unphysical 1s state. In the present study, the SC calculation was carried out also by using the projected Hamiltonian. It can be found that the effect of the unphysical 1s state is negligible. This is because the unphysical state has an energy ($\sim -50$ eV) much lower than the 2s state. Therefore, we do not need to worry about the presence of the unphysical 1s state.

The relation between the principal quantum number $N$ and the energy level $E_{NL}$ is plotted in Fig. 2 for $L = 20, 40, 60$, and
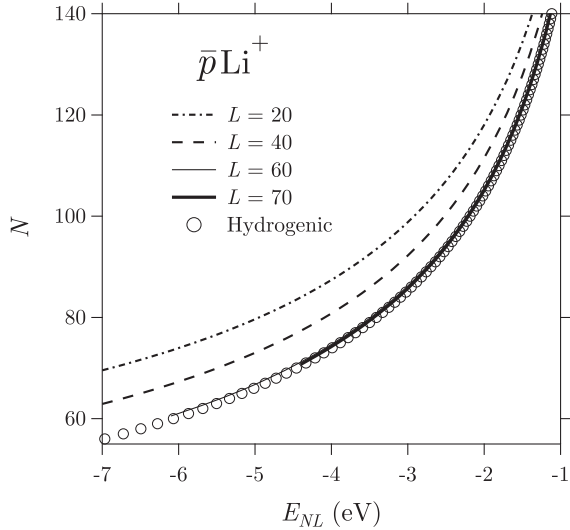
FIG. 2. Principal quantum numbers $N$ plotted against the bound-state energy $E_{NL}$ of $\bar{p}\text{Li}^+$. The hydrogenic formula $E_{NL} = -m_R/(2N^2)$ is also shown.

70. If the $\text{Li}^+$ core can be regarded as a point charge, the energy is given by the hydrogenic formula $-m_R/(2N^2)$. As can be seen in Fig. 2, the hydrogenic formula is applicable for $L \gtrsim 60$ and is no longer useful for low $L \lesssim 40$. The core ($\text{Li}^+$) effect is larger for lower $L$, and the potential $V_{\bar{p}\text{-Li}^+}(R)$ is more attractive than $-1/R$ at small distances [10]. Therefore, the energy $E_{NL}$ for a fixed $N$ decreases with decreasing $L$. As in the case of Rydberg atoms [31], it is interesting to express the energy level in the form $E_{NL} = -m_R/[2(N - \eta_{NL})^2]$, with $\eta_{NL}$ being the quantum defect. Figure 3 shows the quantum defect $\eta_{NL}$ plotted against $N$ for several $L$. As $L$ decreases, the effective potential of $\bar{p} + \text{Li}^+$ becomes deeper and, accordingly, the quantum defect has weaker $N$ dependence [31]. For very high $L$, although the $N$ dependence becomes significant, the quantum defect itself is very small ($\eta_{NL} \ll N$) so that the hydrogenic formula is a very good approximation to the energy level.
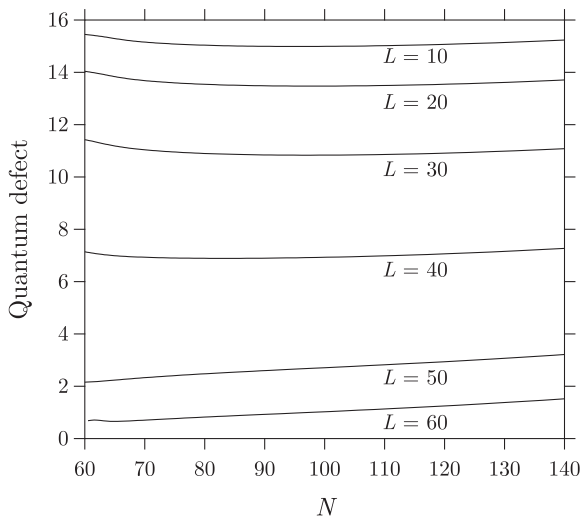


FIG. 3. Quantum defects $\eta_{NL}$ of $\bar{p}\text{Li}^+$ for several $L$ plotted against the principal quantum number $N$.

The procedure of the calculation in the SC method is summarized as follows: (1) The time dependence $R(t)$ is assumed to be the trajectory determined by the adiabatic potential $U_{\text{ad}}(R)$. Then, the time evolution of the wave packet $\psi^{J\lambda}(\mathbf{r},t)$ of the electrons is calculated in quantum mechanics. (2) From the analysis of the outgoing flux of the electrons, the angular-momentum and kinetic-energy distributions of the emitted electrons are calculated. (3) Since the conservation of total angular momentum is properly taken into account, the $L$-state distribution of the capture products can be straightforwardly obtained. (4) By assuming conservation of total energy, one can derive the $(N,L)$-state distribution of the capture products.

### B. Applicability assessment of the present method

Before discussing the results of $\bar{p} + \text{Li}$, we examine the applicability of the present method for calculating the product-state distributions. For this purpose, we consider the capture of negative muons $\mu^-$ by H atoms [i.e., $\mu^- + \text{H} \rightarrow \mu^- p(N,L) + e$], since accurate QM studies of the product-state distributions are available [14,16]. The product $\mu^- p$ in this reaction is called muonic hydrogen, and its energy level is rigorously given by the hydrogenic formula. In the $\mu^- + \text{H}$ system, the interaction is the sum of the pure Coulomb forms.

We examine the approximation assumed in obtaining Eq. (2); namely, that the cross term in the kinetic-energy operators is neglected. (We call it the no-cross-term approximation.) In the present study, the QM calculation based on the $R$-matrix method [16] was carried out for the capture probabilities in $\mu^- + \text{H}$ with use of this approximation. The comparison with the previous accurate $R$-matrix calculation [16] shows that the approximation is reasonably accurate. Since the $\mu^- + \text{H}$ system has a mass ratio of $\mu^-$ to $p$ similar to that of $\bar{p}$ to $\text{Li}^+$, the no-cross-term approximation is expected to be satisfactory also for the $\bar{p} + \text{Li}$ system.

Next, the SC calculation was carried out for the state distributions of the capture products in $\mu^- + \text{H}$. The total angular momenta needed in this case are $J \leqslant 25$ at collision energies $\leqslant 10$ eV. In Figs. 4 and 5, the SC results of the state distributions $F(N)$ and $F(L)$ are compared with the previous QM results obtained by the $R$-matrix method [16] at low energies ($\leqslant 1$ eV) and by the time-dependent method [14] at high energies ($> 1$ eV). We see that the SC method can reasonably reproduce the QM results at all the collision energies of $\leqslant 10$ eV. Although the number $N$ appears to be continuous in the SC calculation, we may draw attention to only its integer value. The present SC method is found to be sufficiently reliable for the detailed investigation of the product-state distributions. For the $\bar{p} + \text{Li}$ system, much larger values of $J$, $N$, and $L$ are involved so that the present SC method is expected to be more appropriate.

## IV. FORMATION OF ANTIPROTONIC LITHIUM

### A. State distribution

First of all, we investigate the energy distribution $F(\epsilon)$ of the emitted electrons in the $\bar{p}$ capture by Li. The results calculated at several collision energies $E$ are shown in Fig. 6. At the low collision energies $E = 0.1$ and $1$ eV, the distributions $F(\epsilon)$ are
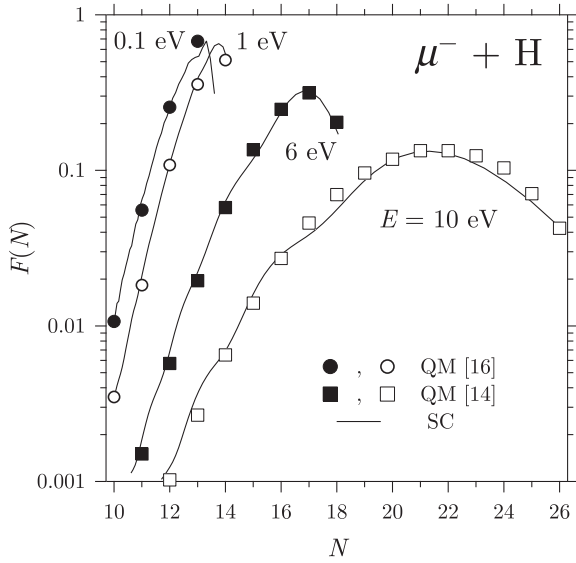
FIG. 4. $N$-state distributions $F(N)$ of $\mu^- p$ produced in the $\mu^-$ capture by H at several collision energies $E$, obtained by the QM [14,16] and the present SC methods.



FIG. 6. Electron-energy distributions $F(\epsilon)$ obtained by the present SC method at several collision energies.

almost the same and have the maximum peak at $\epsilon \sim 0.2$ eV. At high collision energies $E \geqslant 2$ eV, the $E$ dependence becomes recognizable, and the peak position of the distribution shifts toward higher $\epsilon$ with increasing $E$. At all the collision energies considered here, we see that most of the emitted electrons can only have kinetic energies falling within $\epsilon \lesssim 1.5$ eV.

Figure 7 shows the $L$-state distribution of the capture products $\bar{p}\mathrm{Li}^+$. With increasing energy $E$, higher angular momentum states can be produced. At the low energies $E = 0.01$ and $0.1$ eV, the distributions show an abrupt decrease beyond a certain value $L = L_0$ ($L_0 = 32$ and $55$, respectively). This occurs due to the barrier (local maximum) of the effective potential $U_{\mathrm{eff}}(R)$, which can exist for $J \leqslant 70$. [The highest
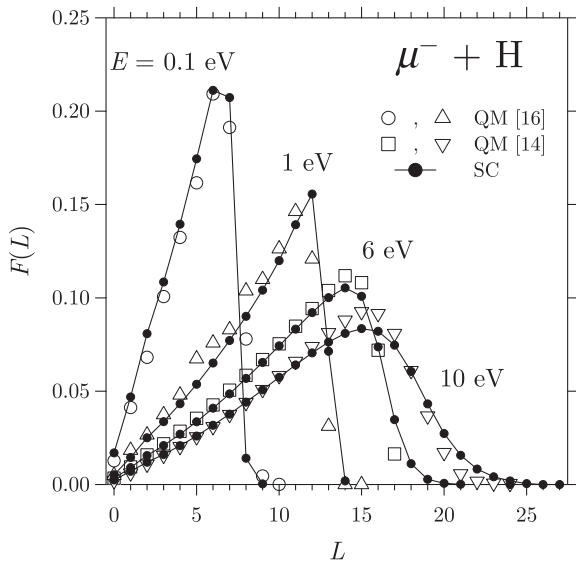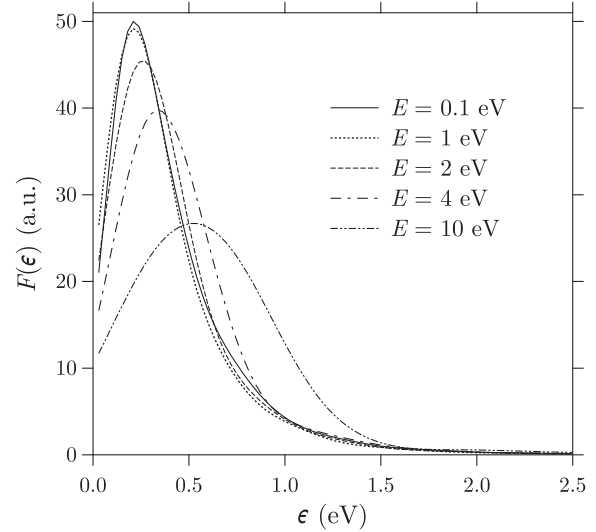
barrier height of $U_{\mathrm{eff}}(R)$ measured from $\mathcal{E}_{\mathrm{Li}}$ is 0.283 eV for $J = 70$.] Let $J_{\max}$ be the maximum total angular momentum such that the barrier height is below a certain collision energy $E$ (cf. orbiting collisions). Then, at this energy $E$, the capture reaction is classically allowed only if $J \leqslant J_{\max}$. Since the electron angular momentum $l$ is always very small, we can roughly assume $L_0 \simeq J_{\max}$ [16]—indeed, $J_{\max} = 33$ for $E = 0.01$ eV and $J_{\max} = 57$ for $E = 0.1$ eV (for reference, the pure polarization potential gives $J_{\max} = 33$ and $59$, respectively). At high energies ($E > 0.283$ eV), there is no such potential barrier effect, and hence the $L$ distributions become entirely smooth.

For each given $L$, the $N$ distribution is shown at $E = 0.1$ eV in Fig. 8. The principal quantum number $N$ takes values up to the maximum $N_{\max}$ determined by Eq. (23) with $\epsilon = 0$. Furthermore, because the energies of the emitted electrons are mostly limited to $\epsilon \lesssim 1.5$ eV (Fig. 6), the capture into the
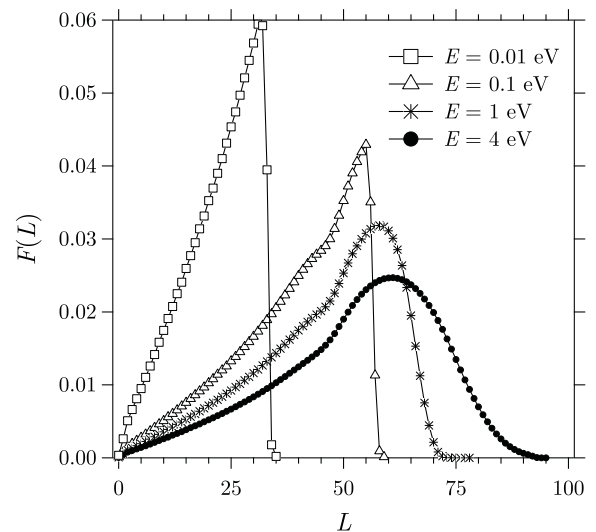


FIG. 5. $L$-state distributions $F(L)$ of $\mu^- p$ produced in the $\mu^-$ capture by H at several collision energies $E$, obtained by the QM [14,16] and the present SC methods.



FIG. 7. $L$-state distributions $F(L)$ obtained by the present SC method at several collision energies.

FIG. 8. $(N,L)$-state distributions $F(N,L)$ for several specified $L$ obtained by the present SC method at the collision energy $E = 1$ eV.
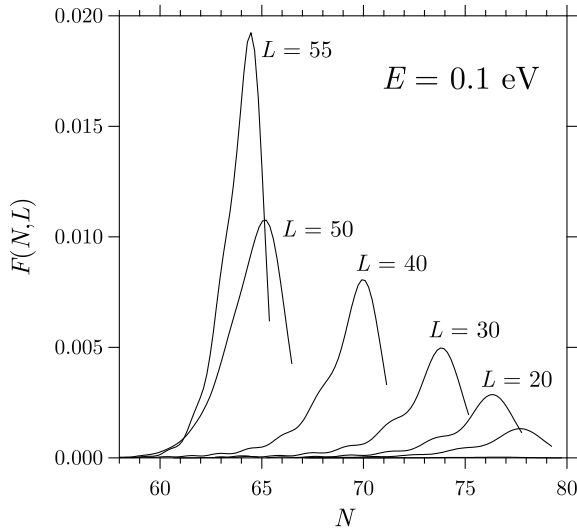


FIG. 9. $(N,L)$-state distributions $F(N,L)$ for several specified $L$ obtained by the present SC method at the collision energy $E = 4$ eV.

$N < 60$ states remains a rare event. As just seen in Fig. 7, the product states span a range $L \lesssim 55$ at $E = 0.1$ eV. For such low $L$, the level structure of $\bar{p}\mathrm{Li}^+$ is quite different from the hydrogenic one (Fig. 2). Accordingly, $N_{\max}$ is strongly dependent on $L$ and is getting larger as $L$ decreases: The assumption of the hydrogenic level provides $N_{\max} \simeq 64$. The peak position $\epsilon \simeq 0.2$ eV in the distribution $F(\epsilon)$ at $E = 0.1$ eV corresponds to $E_{NL} \simeq -5.5$ eV from Eq. (23). We can roughly estimate the peak positions in Fig. 8 by drawing the line $E_{NL} = -5.5$ eV in Fig. 2. For the case of a high collision energy ($E = 4$ eV), the $N$ distribution for each $L$ is shown in Fig. 9. At this energy, as seen in Fig. 7, the states with very high $L$ ($>50$) are abundantly produced. Because the level structure becomes hydrogenic for these high-$L$ values (Fig. 2), most of the major distributions in Fig. 9 are gathered around $N \simeq 115$ and have a similar value of $N_{\max}$ ($\simeq 125$). An interesting feature observed in Fig. 7 is that the distribution profile for low $L$ ($\lesssim 45$) seems to be qualitatively different from that for high $L$ ($\gtrsim 45$) at all the energies $E \geqslant 0.1$ eV. It is evident that this feature reflects the level structure of $\bar{p}\mathrm{Li}^+$. No such feature can be observed in $\mu^- + \mathrm{H}$ (Fig. 5): The level structure of $\mu^- p$ is purely hydrogenic.

Figure 10 shows the $N$-state distribution of the capture products $\bar{p}\mathrm{Li}^+$. In this figure, only the integer values of $N$ are plotted. As the energy $E$ increases, the product states with higher $N$ becomes energetically allowed. The fact that very high states $N > 60$ are always associated with the capture process encourages us to apply the SC method to this problem. As in the case of the $L$ distribution $F(L)$ (Fig. 7), the $N$ distribution also consists of two parts (e.g., $N \lesssim 67$ at $E = 0.1$ eV, $N \lesssim 82$ at $E = 2$ eV, and $N \lesssim 126$ at $E = 4$ eV). From the discussion given above, we can associate the lower-$N$ part of the distribution with the products having the hydrogenic high-$L$ states and the higher-$N$ part with the products having the nonhydrogenic low-$L$ states. The comparison with the $\mu^- + \mathrm{H}$ system is also interesting: In Fig. 4, the "high-$N$ tail" (i.e., the nonhydrogenic part) of the distribution is intrinsically missing. In order to accurately calculate the product-state
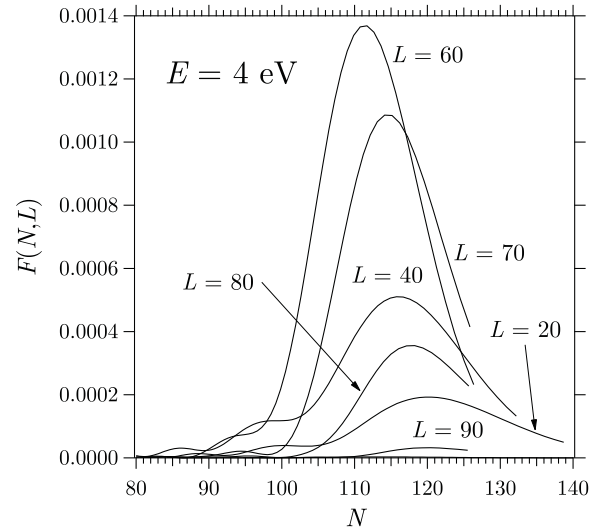
distributions in $\bar{p} + \mathrm{Li}$, one must take account of the fact that the $\bar{p}\mathrm{Li}^+$ atom has a nonhydrogenic level structure.

### B. Total cross section

The total capture cross sections $\sigma$ at collision energies $E = 0.01 - 5$ eV are shown in Fig. 11. The capture cross section for the Li target is much larger than that for the H and He targets [14,15,20] because the $2s$ valence state of Li is very diffuse. At very low energies, the so-called Langevin cross section $\sigma_{\mathrm{L}} = \pi(2\alpha/E)^{1/2}$ can be a measure of the ion-molecule reaction cross section. In Fig. 11, the scaled Langevin cross section $\kappa\sigma_{\mathrm{L}}$ with $\kappa = 0.67$ is plotted, and we see that it agrees well with the present SC cross section at $E \lesssim 0.2$ eV; the factor $\kappa = 0.67$ is smaller than $\kappa = 0.89$ in $\bar{p} + \mathrm{H}$ [20]. If the local maximum of the effective potential $U_{\mathrm{eff}}(R)$ plays no important role (i.e., $E > 0.283$ eV), the adiabatic ionization (AI) model [32] may be more reasonable. However, the AI
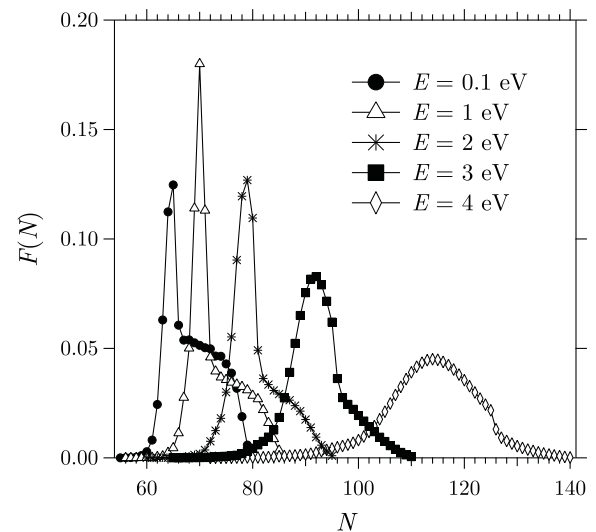


FIG. 10. $N$-state distributions $F(N)$ obtained by the present SC method at several collision energies.
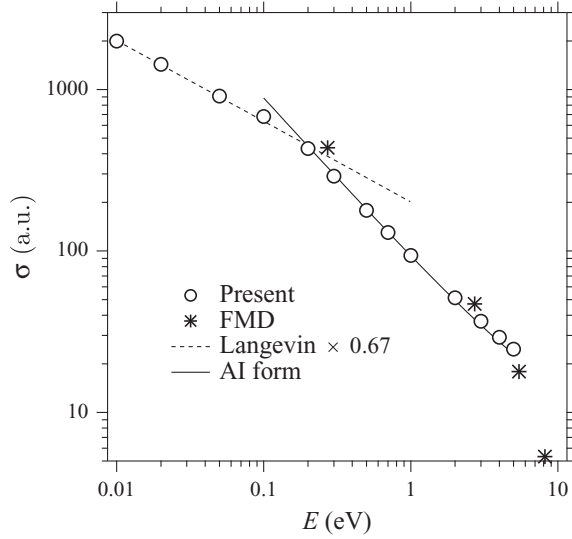
FIG. 11. Total capture cross sections $\sigma$ obtained by the present SC method at collision energies $E = 0.01$ to 5 eV. Also shown are the FMD results [13], the Langevin cross sections multiplied by the factor $\kappa = 0.67$, and the cross sections obtained by assuming the AI form with the fitting parameter $R_0 = 1.3$ a.u.



FIG. 12. Total capture ($\sigma$) and total ionization ($\sigma_{\text{ion}}$) cross sections obtained by the present SC method at collision energies $E = 4$ to 10 eV. The ionization threshold of Li is $I = 5.39$ eV. Total capture cross sections obtained by the FMD method [13] are also shown.

model usually provides too-small capture cross sections [32]. Here, the capture cross section is assumed to have the same form as the AI one:

$$\sigma_{\text{AI}} = \frac{\pi (R_0)^2}{E} [E - U_{\text{ad}}(R_0) + \mathcal{E}_{\text{Li}}], \tag{35}$$

where $R_0$ is treated rather as a fitting parameter: $R_0$ may be regarded as an effective interaction range. In Fig. 11, the result of the AI model with $R_0 = 1.3$ a.u. is shown, and it nicely reproduces the present cross sections at $E \gtrsim 0.2$ eV. As in the case of the $\bar{p} + \text{H}$ system [20], we may offer an empirically fitting formula for $P^J$ vs $R_{\text{TP}}$, with $R_{\text{TP}}$ being the classical turning point in Eq. (9). Using the present SC data, we may have

$$P^J_{\text{fitting}} = [1.08 - 0.493 \exp(1.14 R_{\text{TP}})]$$
$$\times \exp[-0.0237(R_{\text{TP}})^{5.14}], \tag{36}$$

within the error of $\sim 10\%$. This formula is useful for roughly estimating the total capture cross section in $\bar{p} + \text{Li}$ at any energy below the ionization threshold. Equation (36) provides very small probabilities for $R_{\text{TP}} > 3$ a.u. and has the local maximum at $R_{\text{TP}} \simeq 1.1$ a.u., which is slightly smaller than $R_0$ in Eq. (35). Cohen carried out the FMD calculation of the total capture cross sections in $\bar{p} + \text{Li}$ [13]. His results are also shown in Fig. 11. The FMD cross sections at the two lowest energies reported by Cohen are not so different from the present results. However, the applicability of the FMD method at very low energies is problematic because it cannot accurately describe the polarization effect [13].

In the energy range $E = 4$ to 10 eV, the total capture cross sections $\sigma$ are displayed in Fig. 12. The breakup ionization channel is open at energies above the threshold $I = 5.39$ eV. The total ionization cross sections $\sigma_{\text{ion}}$ obtained by using Eq. (34) are also shown in Fig. 12. At collision energies exceeding $E = I$, the capture cross section decreases rapidly,
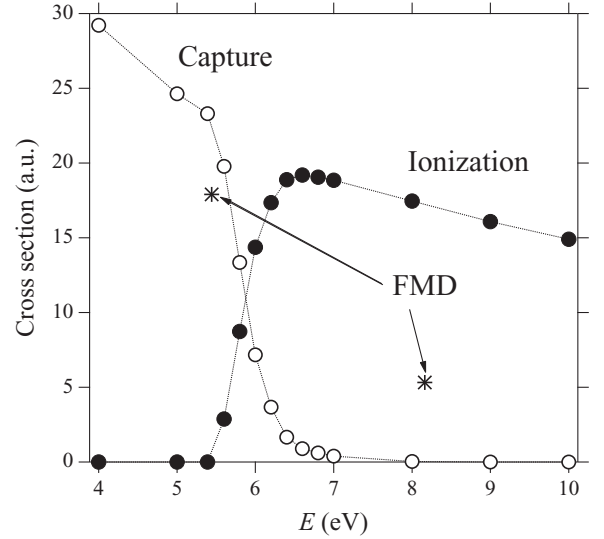
and, competitively, the ionization cross section rises up. Let $\Delta \epsilon$ be the width ($\sim 1.5$ eV) of the distribution $F(\epsilon)$ at $E \simeq I$. It is evident from Eqs. (33) and (34) that the drastic change in the cross sections occurs at energies in a narrow range $(I, I + \Delta \epsilon)$. Since $\Delta \epsilon$ is small, the ionization cross section turns out to take large values even near the threshold ($E \gtrsim I + \Delta \epsilon$); such a feature was reported in a QM study for $\bar{p} + \text{H}$ [33]. The obvious alteration in the behavior of the capture cross section just above the ionization threshold was reported also in the FMD and classical trajectory Monte Carlo (CTMC) calculations for the captures by H and He targets [13,32,34,35]. For heavier targets including Li atoms, however, the FMD calculation shows rather a smooth behavior around the first ionization threshold [13,32]: At the energy $E = 8.16$ eV (0.3 a.u.) in Fig. 12, the FMD capture cross section [13] takes a significantly large value, although the present one is negligibly small. Cohen presumed that multielectron processes were attributable to the smoothness around the first ionization threshold. In the present method, unfortunately, such effects cannot be taken into account. For the $\bar{p}$ capture by He$^+$, the FMD method was found to considerably overestimate the capture cross section [17]. This may suggest that the FMD method is unsuitable for the capture process accompanied by the emission of inner (i.e., strongly bound) electrons. The QM treatment of the electrons is crucial for fruitful discussion on the multielectron effect.

## V. LONG-LIVED ANTIPROTONIC ATOMS

### A. Antiprotonic Lithium

The $\bar{p}\text{Li}^+$ atom has a decay channel due to the Auger transition; that is,

$$\bar{p}\text{Li}^+(N,L) \to \bar{p}\text{Li}^{2+}(N',L') + e. \tag{37}$$

Here, we discuss the stability against this Auger channel. Figure 13 shows the effective potentials of the $\bar{p} + \text{Li}^+$ and
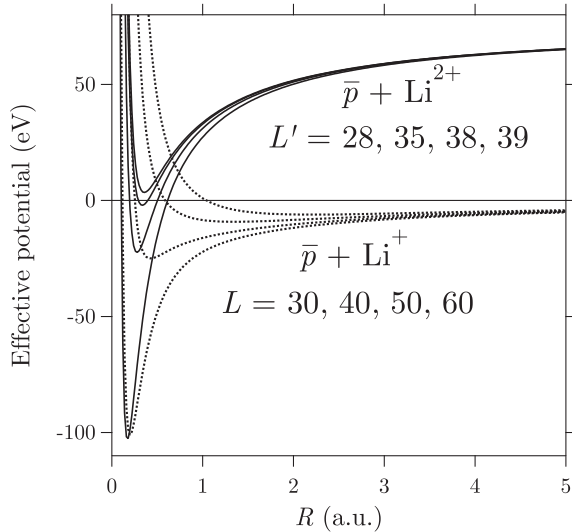
FIG. 13. Effective potentials of $\bar{p} + \mathrm{Li}^{2+}$ for the relative angular momenta $L' = 28, 35, 38$, and 39 (from bottom up) and of $\bar{p} + \mathrm{Li}^+$ for $L = 30, 40, 50$, and 60 (from bottom up). The BO electronic energies of these systems are taken from Ahlrichs *et al.* [10].
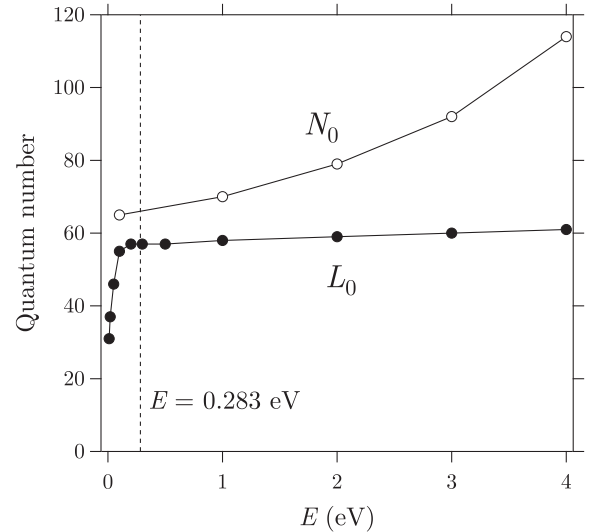


FIG. 14. Quantum numbers $L_0$ and $N_0$ which give the maximum values of the distributions $F(L)$ and $F(N)$, respectively. Shown by the vertical dotted line is the energy (0.283 eV) corresponding to the barrier height of the effective potential $U_{\mathrm{eff}}(R) - \mathcal{E}_{\mathrm{Li}}$ for $J = 70$.

$\bar{p} + \mathrm{Li}^{2+}$ systems obtained by using the data of Ahlrichs *et al.* [10]. We can see that the $\bar{p} + \mathrm{Li}^{2+}$ effective potential is everywhere positive for $L' \geqslant 39$, and thus that $L'$ must be $\leqslant 38$ in Eq. (37) for any $L$. This means that, if the state of $\bar{p}\mathrm{Li}^+$ is $L \geqslant 39$, then the angular momentum change $\Delta L = |L' - L|$ is $\Delta L \geqslant L - 38$. Since $\Delta L$ is roughly equal to the angular momentum $l'$ of the Auger electron, the Auger transition should be strongly suppressed for $L \gg 39$. The minimum of the $\bar{p} + \mathrm{Li}^{2+}$ effective potential for $L' = 28$ is lower than the minimum of the $\bar{p} + \mathrm{Li}^+$ one for $L = 30$. Therefore, it is easily inferred that the $\bar{p}\mathrm{Li}^+$ states with $L \lesssim 30$ can have large Auger decay rates. If the condition that the $\bar{p}\mathrm{Li}^+(N,L)$ state be measurable within the lifetime can be satisfied by $\Delta L > 2$, as in the case of $\bar{p}\mathrm{He}^+$ [1,6], the states with $L > 40$ are measurable in $\bar{p}\mathrm{Li}^+$. Figure 13 further shows that the Franck-Condon overlap between the two states to be connected by the Auger transition is very small if $L \gtrsim 50$. Also in this sense, the Auger transition would become practically negligible for $L \gtrsim 50$. These conclusions hold for any value of $N \geqslant L$, and are not limited to the near-circular states.

Next, we examine the stability of the produced $\bar{p}\mathrm{Li}^+$ state in the capture reaction. Figure 14 shows the quantum numbers $L_0$ and $N_0$ which give the maximum values of the distributions $F(L)$ and $F(N)$, respectively. From the discussion in the previous section, we can assume $L_0 \simeq J_{\max}$ if $E < 0.283$ eV. It follows that $L_0 \to 0$ as $E \to 0$. However, if $E > 0.02$ eV, we have $L_0 > 40$ so that most of the produced $\bar{p}\mathrm{Li}^+$ turn out to be fairly stable against the Auger process. Shimamura *et al.* [12] suggested that the Auger transition can be suppressed always for $N > 45$ unless $L \ll N$. In contrast to the $L$ distribution, the product states are always $N \gtrsim 60$ regardless of the energy $E$. Furthermore, we can see in Figs. 8 and 9 that the capture into low-$L$ states results in a relatively large amount of the products having rather very-high-$N$ states. In conclusion, long-lived $\bar{p}\mathrm{Li}^+$ is expected to be effectively produced in almost all the capture processes except at extremely low energies. As

was suggested in previous studies [10–12], the formation of the long-lived antiprotonic atoms occurs indeed far more frequently in the $\bar{p} + \mathrm{Li}$ collisions than in $\bar{p} + \mathrm{He}$. Also, for the targets of alkali-metal atoms other than Li, the efficient formation of long-lived antiprotonic atoms can be expected by the same token. The present result strongly encourages the performance of spectroscopic studies of antiprotonic lithium in the same way as was done for antiprotonic helium [1,3], although no delayed annihilation of $\bar{p}$ was experimentally observed in solid Li metal [36]: The capture dynamics may differ considerably between the gas phase and the metal phase for alkali-metal atoms.

### B. Antiprotonic helium

Finally, we consider the $\bar{p}\mathrm{He}^+$ atom. Figure 15 shows the effective potentials of the $\bar{p} + \mathrm{He}^+$ and $\bar{p} + \mathrm{He}^{2+}$ systems obtained by using the data of Shimamura [22]. It is interesting that the potential feature of Fig. 15 is very similar to that of Fig. 13. The $\bar{p} + \mathrm{He}^{2+}$ effective potential is always above the $\mathrm{He}^+(1s)$ energy for $L' \geqslant 38$. We can see that the Auger transition is strongly suppressed for the $\bar{p}\mathrm{He}^+$ states with $L \gg 38$ and is promoted when $L \lesssim 30$.

In $\bar{p}$ capture by He, Tong *et al.* [15] provided detailed information on the product-state distribution at a single collision energy of 10 eV and show that the dominantly populated $(N, L)$ states of $\bar{p}\mathrm{He}^+$ are $N \simeq 40 \simeq 45$ and $L \simeq 25-40$. As the collision energy decreases, those corresponding $L$ should become small. Therefore, the $\bar{p}\mathrm{He}^+$ states produced in the capture would be mostly unstable due to the Auger transition if the collision energy is much lower than 10 eV. For this reason, only the near-circular states, which are produced at a rate of only a few percent in the capture by He, can play an important role in the measurements of $\bar{p}\mathrm{He}^+$ [1,9]. It should be mentioned here that Tong *et al.* [15] employed the no-cross-term approximation, in the same way as introduced in Eq. (2). This approximation can be validated for heavy mass
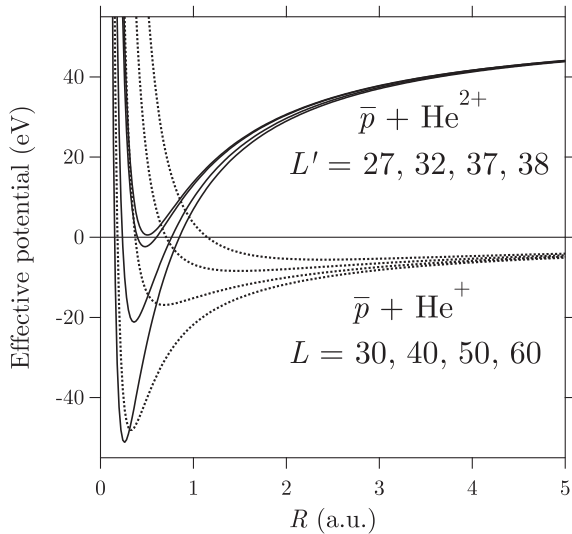
FIG. 15. Effective potentials of $\bar{p} + \mathrm{He}^{2+}$ for the relative angular momenta $L' = 27,32,37$, and 38 (from bottom up) and of $\bar{p} + \mathrm{He}^+$ for $L = 30,40,50$, and 60 (from bottom up). The energies are measured from the $\mathrm{He}^+(1s)$ level. The BO electronic energies of $\bar{p} + \mathrm{He}^+$ are taken from Shimamura [22].

targets like Li atoms (cf. Sec. III B), but its applicability to the He target is uncertain: The no-cross-term approximation is indeed poor with regard to the low-lying prominent resonances in $\bar{p} + \mathrm{He}^+$ collisions [17] although resonances are absent in $\bar{p} + \mathrm{He}$. A further theoretical study of the $\bar{p}$ capture by He is needed.

If the He atom is in a metastable state such as $2\,^3S$ (its binding energy being 4.77 eV), then all the conditions for the capture and subsequent Auger processes in the case of $\bar{p} + \mathrm{He}(2\,^3S)$ become analogous to those in $\bar{p} + \mathrm{Li}$. Matching

the $\bar{p}\mathrm{He}^+$ energy to the $2\,^3S$ level of He leads to the most probable $N \sim 65$, and it indeed follows that the long-lived $\bar{p}\mathrm{He}^+$ atoms having $L \gg 38$ can be produced in the capture. The potential observability of such high-$L$ states was also suggested by Tolstikhin *et al.* [37]. On the analogy of the present result for $\bar{p} + \mathrm{Li}$, we can naturally expect that the states with $L \gg 38$ are produced abundantly in $\bar{p} + \mathrm{He}(2\,^3S)$. Thus, $\bar{p}$ capture will be an efficient formation process of long-lived $\bar{p}\mathrm{He}^+$ if the metastable $\mathrm{He}(2\,^3S)$ atom is chosen as the target.

## VI. CONCLUSION

The SC method has been developed for the calculations of not only the total cross sections but also the product-state distributions in the capture of antiprotons by atoms. The applicability of the present method has been demonstrated for the capture of negative muons by H atoms: the accurate QM calculation was already performed for this system. By using the present method, one can calculate the cross sections for the capture and ionization separately even at energies above the ionization threshold. It has been found that the $\bar{p}$ capture by Li atoms occurs to form antiprotonic lithium atoms $\bar{p}\mathrm{Li}^+$ mostly in the states with $L \gtrsim 50$ (if $E \gtrsim 0.1$ eV) and $N > 60$. Therefore, most of the $\bar{p}\mathrm{Li}^+$ atoms produced in the capture exhibit sufficient stability against Auger transition and can be observed in experiments as long-lived states. Noting similarities between $\bar{p} + \mathrm{Li}$ and $\bar{p} + \mathrm{He}(2S)$, one can also expect efficient formation of long-lived antiprotonic helium atoms $\bar{p}\mathrm{He}^+$ in $\bar{p}$ capture by $\mathrm{He}(2S)$ atoms.

## ACKNOWLEDGMENTS

[1] T. Yamazaki, N. Morita, R. Hayano, E. Widmann, and J. Eades, Phys. Rep. **366**, 183 (2002).
[2] M. Hori, Phys. Rep. **403-404**, 337 (2004).
[3] R. S. Hayano, M. Hori, D. Horváth, and E. Widmann, Rep. Prog. Phys. **70**, 1995 (2007).
[4] G. T. Condo, Phys. Lett. **9**, 65 (1964).
[5] J. E. Russell, Phys. Rev. Lett. **23**, 63 (1969).
[6] V. I. Korobov and I. Shimamura, Phys. Rev. A **56**, 4587 (1997).
[7] J. Révai and A. T. Kruppa, Phys. Rev. A **57**, 174 (1998).
[8] E. Widmann *et al.*, Phys. Rev. A **53**, 3129 (1996).
[9] J. S. Briggs, P. T. Greenland, and E. A. Solov'ev, J. Phys. B **32**, 197 (1999).
[10] R. Ahlrichs, O. Dumbrajs, H. Pilkuhn, and H. G. Schlaile, Z. Phys. A **306**, 297 (1982).
[11] J. Révai and V. B. Belyaev, Phys. Rev. A **67**, 032507 (2003).
[12] I. Shimamura, M. Kimura, and Y. Korenman, XXI ICPEAC, *Abstracts of Contributed Papers* (Sendai, Japan, 1999), p. 446.
[13] J. S. Cohen, Phys. Rev. A **69**, 022501 (2004).
[14] X. M. Tong, T. Shirahama, K. Hino, and N. Toshima, Phys. Rev. A **75**, 052711 (2007).

[15] X. M. Tong, K. Hino, and N. Toshima, Phys. Rev. Lett. **101**, 163201 (2008).
[16] K. Sakimoto, Phys. Rev. A **81**, 012511 (2010).
[17] K. Sakimoto, Phys. Rev. A **82**, 012501 (2010).
[18] N. H. Kwong, J. D. Garcia, and J. S. Cohen, J. Phys. B **22**, L633 (1989).
[19] K. Sakimoto, J. Phys. B **34**, 1769 (2001).
[20] K. Sakimoto, Phys. Rev. A **65**, 012706 (2001); **66**, 032506 (2002).
[21] G. Peach, H. E. Saraph, and M. J. Seaton, J. Phys. B **21**, 3669 (1988).
[22] I. Shimamura, Phys. Rev. A **46**, 3776 (1992).
[23] K. Sakimoto, J. Phys. B **33**, 3149 (2000).
[24] H. A. Behte and E. E. Salpeter, in *Quantum Mechanics of One-And Two-Electron Atoms* (Plenum Publishing Corporation, New York, 1977), p. 166.
[25] B. H. Choi and R. T. Poe, Phys. Rev. A **16**, 1821 (1977).
[26] D. E. Manolopoulos and M. H. Alexander, J. Chem. Phys. **97**, 2527 (1992).
[27] N. Balakrishnan, C. Kalyanaraman, and N. Sathyamurthy, Phys. Rep. **280**, 79 (1997).

[28] S. Yu. Ovchinnikov and J. H. Macek, Phys. Rev. A **71**, 052717 (2005).

[29] G. M. Stacey, Proc. Phys. Soc. London **88**, 897 (1966).

[30] O. H. Crawford, Proc. Phys. Soc. **91**, 279 (1967).

[31] M. J. Seaton, Rep. Prog. Phys. **46**, 167 (1983).

[32] J. S. Cohen, Rep. Prog. Phys. **67**, 1769 (2004).

[33] K. Sakimoto, Phys. Rev. A **70**, 064501 (2004).

[34] J. S. Cohen, Phys. Rev. A **27**, 167 (1983).

[35] D. R. Schultz, P. S. Krstić, C. O. Reinhold, and J. C. Wells, Phys. Rev. Lett. **76**, 2882 (1996).

[36] E. Widmann *et al.*, Phys. Rev. A **51**, 2870 (1995).

[37] O. I. Tolstikhin, S. Watanabe, and M. Matsuzawa, Phys. Rev. A **54**, R3705 (1996).